Molecular Biology of the Cell
Vol. 18, 1595–1608, May 2007

The Biogenesis of the Golgi Ribbon: The Roles of Membrane Input from the ER and of GM130[D] [V]

Pierfrancesco Marra,* Lorena Salvatore, Alexander Mironov Jr.,† Antonella Di Campli, Giuseppe Di Tullio, Alvar Trucco, Galina Beznoussenko, Alexander Mironov, and Maria Antonietta De Matteis

Department of Cell Biology and Oncology, Consorzio Mario Negri Sud, 66030 Santa Maria Imbaro, Chieti, Italy

Submitted October 3, 2006; Revised November 29, 2006; Accepted February 6, 2007
Monitoring Editor: Benjamin Glick

The Golgi complex in mammalian cells forms a continuous ribbon of interconnected stacks of flat cisternae. We show here that this distinctive architecture reflects and requires the continuous input of membranes from the endoplasmic reticulum (ER), in the form of pleiomorphic ER-to-Golgi carriers (EGCs). An important step in the biogenesis of the Golgi ribbon is the complete incorporation of the EGCs into the stacks. This requires the Golgi-matrix protein GM130, which continuously cycles between the *cis*-Golgi compartments and the EGCs. On acquiring GM130, the EGCs undergo homotypic tethering and fusion, maturing into larger and more homogeneous membrane units that appear primed for incorporation into the Golgi stacks. In the absence of GM130, this process is impaired and the EGCs remain as distinct entities. This induces the accumulation of tubulovesicular membranes, the shortening of the cisternae, and the breakdown of the Golgi ribbon. Under these conditions, however, secretory cargo can still be delivered to the Golgi complex, although this occurs less efficiently, and apparently through transient and/or limited continuities between the EGCs and the Golgi cisternae.

INTRODUCTION

The Golgi complex (GC) in mammals is organized in the form of a continuous ribbon-like organelle that is made up of interconnected stacks of flat cisternae that are positioned close to the centrosome. The whys and wherefores of this distinctive architecture and positioning are not completely understood, and many basic aspects of the morphofunctional organization of the GC remain to be clarified.

Among these, a key issue is how the GC achieves its structural organization and maintains its identity under the very variable conditions of membrane load. Indeed, the GC can absorb massive membrane input from the endoplasmic reticulum (ER) that under certain conditions can equal or even exceed the surface area of the Golgi stacks themselves (Mironov *et al.*, 2001). These incoming membranes arrive at the GC as pleiomorphic ER-to-Golgi carriers (EGCs), which are large tubulovesicular structures that vary in size from 60 to 80 nm up to 1 μm (Presley *et al.*, 1997; Scales *et al.*, 1997; Mironov *et al.*, 2003). At present, it is not clear how these highly pleiomorphic membrane units are efficiently incorporated into the Golgi ribbon.

These uncertainties are due in part to the limits of spatial resolution of current morphological approaches, as it remains difficult to resolve events that occur at the interface between EGCs and the GC in the pericentriolar area, an area that is intrinsically complex because of the concentration of membranes of different natures. Recently, however, the microtubule disrupting agent nocodazole (NZ) has been used to "simplify" the organization of the Golgi ribbon into disconnected and peripheral, but functional, ministacks; EGCs enter these ministacks by both forming new cisternae at the *cis* pole and by expanding the pre-existing cisternae (Trucco *et al.*, 2004). However, the molecular mechanisms and the structural intermediates that operate in this transition from tubulovesicular pleiomorphic membranes (the EGCs) to regular flat cisternae remain to be defined.

One of the proteins involved in the transition from vesicular-type membranes into cisternal membranes is GM130 (Nakamura *et al.*, 1997), a member of the family of coiled-coil golgins that includes, among others, p115, GRASP65, and giantin. These proteins can form a complex that has been proposed to act as a molecular tether between vesicles and acceptor membranes before fusion. Indeed, the tethering properties of this protein complex were originally deduced from in vitro studies where GM130 was shown to be required for the reformation and lengthening of the Golgi cisternae, starting from mitotic Golgi vesicles (Shorter and Warren, 1999), and for the docking of COPI vesicles to acceptor Golgi cisternae (Sonnichsen *et al.*, 1998). Along the same lines, interfering with GM130 has been seen to result in an accumulation of vesicular membranes and an inhibition of ER-to-Golgi transport (Alvarez *et al.*, 2001). At odds with these observations, it has been proposed recently that the main tethering activity of GM130 is between neighboring

This article was published online ahead of print in *MBC in Press* (http://www.molbiolcell.org/cgi/doi/10.1091/mbc.E06–10–0886) on February 21, 2007.

[D] [V] The online version of this article contains supplemental material at *MBC Online* (http://www.molbiolcell.org).

Present addresses: * Section of Cell and Molecular Biology, Institute of Cancer Research, Chester Beatty Laboratories, 237 Fulham Road, London SW3 6JB, United Kingdom; † Electron Microscopy Unit, Faculty of Life Sciences, Stopford Building, University of Manchester, Oxford Road, Manchester, M139PT, United Kingdom.

Address correspondence to: Maria Antonietta De Matteis (dematteis@negrisud.it) or Alexander Mironov (mironov@negrisud.it).

Abbreviations used: CHX, cycloheximide; EGCs, ER-to-Golgi carriers; GC, Golgi complex; KDELR, KDEL receptor; N309, an antibody directed against the N309 aa of GM130.

cisternae rather than between vesicular membranes and cisternae (Puthenveedu *et al.*, 2006). Finally, and in apparent contrast with the concept that GM130 has a role in controlling the function or the structure of the GC in mammals, injection of anti-GM130 antibody causes no apparent defects in the organization of the GC (Puthenveedu *et al.*, 2001) and randomly mutagenized Chinese hamster ovary (CHO) cells that do not express GM130 (ldlG cells) have an apparently normal GC at permissive temperatures (Malmstrom and Krieger, 1991; Vasile *et al.*, 2003).

Thus, divergent and contrasting interpretations of the role of GM130 are present in the literature, with the result that the precise mode and site of action of GM130, the prototype "Golgi matrix" protein, remain to be determined. These divergences mainly depend on the nature and time frame of action of the different approaches used to interfere with GM130 and on the resolution power of the different studies.

Here, we have combined four independent knockout approaches with in-depth functional and ultrastructural analyses to distil out the primary effects of the GM130 knockout from secondary effects and adaptive cell responses and thus to map its site of action in the secretory pathway.

MATERIALS AND METHODS

Reagents and Antibodies

All chemical reagents were of analytical grade or higher and purchased from Sigma-Aldrich (Saint Louis, MO), unless otherwise specified. The polyclonal N309 anti-GM130 antibody was generated using a fusion protein between GST and the first 309 amino acids of human GM130 (N309-GST) and was affinity purified. Anti-G95, anti-giantin, and anti-p115 antibodies were prepared as previously described (Fritzler *et al.*, 1993; Marra *et al.*, 2001); the monoclonal anti-giantin antibody was provided by H. P. Hauri (University of Basel, Basel, Switzerland); the monoclonal anti-KDEL receptor antibody was from StressGen Biotechnologies (Victoria, BC, Canada); Alexa 488 goat anti-mouse and anti-rabbit IgG (H+L), from Molecular Probes (Eugene, OR); anti-mouse and anti-rabbit Cy3-conjugated, from Sigma-Aldrich; and FluoroLink™5-labeled goat anti-rabbit and anti-mouse IgG (H+L), from Amersham Biosciences (Piscataway, NJ).

Cell Transfection

COS7 and NRK cells were transfected with the Trans Fast Transfection Reagent (Promega, Madison, WI), according to manufacturer's instructions. HeLa cells were transfected with the Fugene 6 Transfection Reagent (Roche, Indianapolis, IN), according to manufacturer's instructions. The cells were treated 16 h after transfection.

DNA Constructs

The full-length human GM130 constructs, GFP-GM130 and the truncated constructs of human GM130, were as previously described (Marra *et al.*, 2001). The full-length human LDR construct, GFP-LDLR was a generous gift from Enrique Rodriguez-Boulan (Cornell University, New York, NY).

RNA Interference

HeLa cells were transfected with 40 pmol RNA duplexes targeting three different sequences of hGM130 (AACCCTGAGACAACCACTTCT, AAGTTAGAGATGACGGAACTC, and ATGAGAACATGGAGATCACC; Preisinger *et al.*, 2004, ; siACE-RNAi Option C from Dharmacon Research, Lafayette, CO) using oligofectamine (Invitrogen, Carlsbad, CA), according to the manufacturer's protocol. For the control, HeLa cells were treated with identical concentrations of luciferase small interfering RNAs (siRNAs; Dharmacon, Perbio Science France SA, Brebières, FR). At 48/72/96 h after the initial siRNA treatment, the cells were directly processed for immunofluorescence and for biochemical analysis, infected with ts045VSV, or labeled with [^{35}S]methionine and assayed for VSVG transport.

Immunofluorescence

All of the cell types were processed as previously described (Godi *et al.*, 1999). For confocal imaging, the samples were examined under a Zeiss LSM 510 confocal microscope (LSCM; Thornwood, NY). Optical sections were obtained with a 63× oil immersion objective, at a definition of 1024 × 1024 pixels, with a pinhole diameter of 1 Airy unit for each emission channel. Quantification of colocalization was carried out as previously described (Marra *et al.*, 2001).

Electron Microscopy, Correlative Light Immunoelectron Microscopy, and Electron Tomography

Human fibroblasts (HFs) and COS7 cells were grown on glass-bottomed MatTek slides (Ashland, MA) with a grid. At different times after injection, the samples were processed for correlative light immunoelectron microscopy (CLEM) as described in the Supplementary Material. Tomograms were made from 160-nm-thick sections from a single axis of −65 to +65° rotation in 1° increments. The tomograms of the Golgi area were produced using the IMOD software package. Three-dimensional reconstruction was carried out after delineation of the membranes using the same software. Vesicles were represented by the software-generated spheres with the center in the center of the vesicles. There were two types of vesicles, of 50–60- and 80–90-nm diameters. A structure was designated as a vesicle when on the first and last virtual sections there were no more signs of membranous connections with adjacent structures.

Morphometric analysis was performed using the Soft Imaging System software (Münster, Germany). Volume and surface densities of membranous structures were estimated by point and intersection counting with standard morphometry package grids. The sizes of the EGCs and the lengths of the Golgi cisternae were measured with a ruler tool. In serial-section analysis, we defined the "stack coalescence" as a situation where two apparently distinct stacks on one section became one stack on the next section. The number of these "stack coalescence" events was related to the number of stacks in the sections.

Analysis of Cargo Transport and Glycosylation

Analysis of VSVG transport was performed in cells infected with the ts045 VSV at 32°C for 45 min, with an incubation at 40°C for 2 h, and then either shifted to 32°C for different times or further incubated at 15°C for 2 h (to accumulate protein in the intermediate compartment), before being shifted to 32°C for different times. At the end of the incubations, the cells were fixed and processed for immunofluorescence.

LdlG cells are temperature sensitive (nonpermissive temperature, 39.5°C); therefore, ldlG cells (and control CHO cells) were infected with VSV for 1 h at 32°C and then placed at 32°C in the presence of cycloheximide (CHX) for 3 h. The cells were then placed at 15°C in the absence of CHX for 2 h. Finally, the cells were shifted to 32°C for the indicated times. Quantification of VSVG transport was performed by analyzing the immunostaining patterns of at least 200 cells from three independent experiments.

The posttranslational processing of the LDL receptor (LDLR) was assessed in CHO and ldlG cells transfected with green fluorescent protein (GFP)-LDLR. The cells were pulse-labeled for 10 min with [^{35}S]methionine, chased for the indicated times, and lysed. The cell lysates were immunoprecipitated with the anti-GFP antibody and subjected to SDS-PAGE.

The transport and glycosylation of VSVG was assessed by evaluating the acquisition of resistance to Endo-H treatment, the sensitivity to neuraminidase treatment, and cell-surface biotinylation of [^{35}S]methionine-labeled VSVG, as previously described (Buccione *et al.*, 1996; Godi *et al.*, 1998). Of note, all of these experiments with ldlG cells and control CHO cells were carried out at the permissive temperature (32°C). Where indicated, the glycosylation state of endogenous HCAM was also assessed by treating cell lysates with Endo-H and/or Endo-H and neuraminidase and assessing the shift of the band after a Western blotting immunoassay for HCAM with a specific mAb. Lectin staining was performed according to Puthenveedu *et al.* (2006) using either Alexa Fluor 488-lectin GSII (specifically binds terminal *N*-acetyl-D-glucosamine) or *Sambucus nigra* fluorescein-lectin (SNAI, specifically binds sialic acid attached to terminal galactose in an α-2,6 linkage).

RESULTS

Formation and Maintenance of the Golgi Ribbon Depend on Continuous Input of Membranes from the ER

Different subcompartments of the GC can vary in volume according to their rates of membrane input and output (Griffiths *et al.*, 1989; Clermont *et al.*, 1993; Morin-Ganet *et al.*, 2000); however, it is unclear how this flux of membranes impacts on the organization of the Golgi ribbon itself. To address this issue, different experimental conditions were set up to interrupt the arrival of EGCs at the GC and to analyze the effects of this block (and of its removal) on the ultrastructure of the GC. Initially, human fibroblasts (HFs) were treated with CHX for 3 h to block the synthesis of secretory cargo and, as a consequence, its transport to the GC. The GC, remained near to the centrosome in CHX-treated cells, but underwent extensive fragmentation, as seen by the increase in the number of distinct fluorescent units within the Golgi mass (Figure 1, A, B, and E).

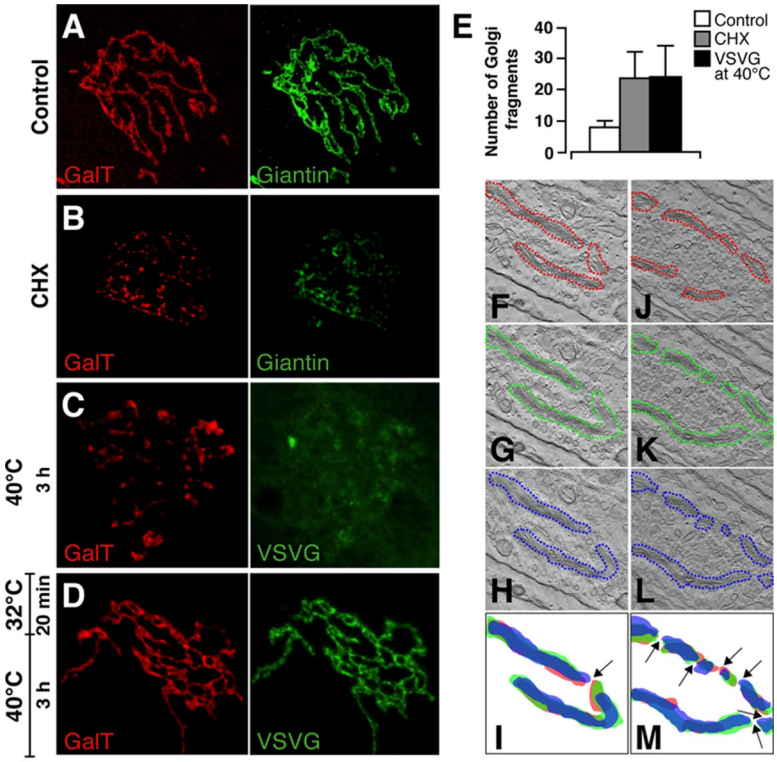

Figure 1. Fragmentation of the Golgi ribbon in the absence of membrane input from the ER. (A) At steady state at 37°C, the distribution patterns of GalT (red) and giantin (green) show a continuous reticulum in HFs. (B) After CHX treatment for 3 h, these Golgi-resident proteins reveal the GC as fragmented into discrete elements. (C) With VSV-infected cells incubated at 40°C for 3 h, fixed, and stained for GalT (red) and VSVG (green), the staining pattern of GalT is again fragmented, and VSVG is retained in the ER. (D) When cells in C were then incubated at 32°C for 20 min, fixed, and stained for GalT (red) and VSVG (green), GalT reveals a continuous ribbon, and VSVG is transported to the GC. (E) Quantitation of GC fragmentation as shown in A–C, showing number of isolated GalT-labeled structures seen under LSCM using the *Z*-stacking procedure (after background subtraction). (F–M) HFs were infected with VSV, kept at 40°C for 3 h to accumulate VSVG in the ER (F–M). They were then either fixed (J–M) or placed at 15°C to accumulate VSVG in the intermediate compartment for 15 min and finally shifted to 40°C to allow VSVG accumulated in the intermediate compartment to move through the Golgi for 8 min (F–I). The cells were then processed for electron tomography. Cells with similarly oriented GC are shown. Superimpositions of Golgi profiles (red) of the first (red), 15th (green), and the 31st (blue) virtual serial sections from the same tomogram are shown. Arrows indicate the breakpoints in the ribbon. Quantitative analysis showed that the number of the ribbon breakpoints is 2.5-fold higher in cells incubated at 40°C. Bar, 2 μm (A); 0.7 μm (C).

A similar fragmentation of the GC was seen in HFs infected with ts045VSV, when the transport of VSVG from the ER to the GC was blocked by placing the cells at 40°C (Figure 1, C and E). This temperature block is known to induce a generalized inhibition of COPII-dependent exit of cargo from the ER (Aridor *et al.*, 1999, 2001; Trucco *et al.*, 2004) due to the sequestering of the export machinery by the ER-arrested VSVG, by far the most abundant neosynthesized protein under these conditions. At the EM level, the block of input from the ER induced the disappearance of the continuous Golgi ribbon and its partial conversion into isolated, but centrally located, Golgi "ministacks" (Figure 1, J–M). Of note, these stacks appeared devoid of their highly perforated *cis*-most cisternae.

To determine the effects of the resumption of transport on the organization of the GC, after this 40°C temperature block, the VSV-infected HFs were placed at 32°C for 20 min, to allow VSVG to be transported to the GC. After the release of the block, the continuity of the Golgi elements appeared completely restored (Figure 1, D–I).

This thus established a correlation between the ongoing input of membranes from the ER into the GC and the presence of an intact Golgi ribbon, which indicates that the incorporation of EGCs into the GC is a necessary element to establish and maintain this lateral continuity between adjacent stacks.

The Incorporation of EGCs into the Golgi Stacks Requires a GM130-based Molecular Machinery

The visualization of the incorporation of EGCs into the Golgi stacks is hampered by the complexity of the structure of the Golgi ribbon and its position in the pericentriolar area. One way to circumvent these difficulties is to induce the dispersal of the Golgi ribbon into peripheral ministacks by using NZ (Trucco *et al.*, 2004). As suggested by our previous observations (Marra *et al.*, 2001), GM130 has an important role precisely at the interface between the pre-Golgi membranes and the Golgi stacks. Thus we decided to assess its role in mediating the incorporation of EGCs into the stacks more directly by studying this process in NZ-treated control and GM130-devoid cells. LdlG cells are a temperature-sensitive and conditional-lethal mutant cell line that was obtained from CHO cells by radiation suicide (Malmstrom and Krieger, 1991). At their nonpermissive temperature of 39.5°C, the GC is disassembled and secretion is blocked, whereas at the permissive temperature of 34°C, the structure of the GC appears normal; at both temperatures, ldlG cells have no detectable levels of GM130 (Malmstrom and Krieger, 1991; Vasile *et al.*, 2003). We therefore investigated ER-to-Golgi trafficking in ldlG cells at their permissive temperature, in comparison with wild-type CHO cells and ldlG cells expressing exogenous GFP-GM130.

These cells were thus infected with VSV, treated with NZ for 3 h, and then shifted to 15°C for 2 h (to accumulate VSVG in the EGCs), before being placed at 34°C for 15 min (to allow the transport of the EGCs to the Golgi stacks) and processed for EM. The surface areas of the EGCs, Golgi cisternae, and vesicles plus tubules in the peri-Golgi zone were estimated according to Trucco *et al.* (2004).

At steady state in CHO cells, the surface area of the Golgi cisternae was more than fivefold greater than that of the EGCs (Figure 2). After the 15°C block, greatly enlarged EGCs appeared and the surface area of the cisternae decreased by 30%, becoming lower than that of the EGCs. Neither intercisternal connections nor a typical highly perforated *cis*-most cisterna were seen at this time. Within 15 min of the release of the block, the EGCs significantly decreased in surface area, whereas that of the cisternae increased to a corresponding extent. At the same time, tubular interconnections between successive cisternae and the *cis*-

A

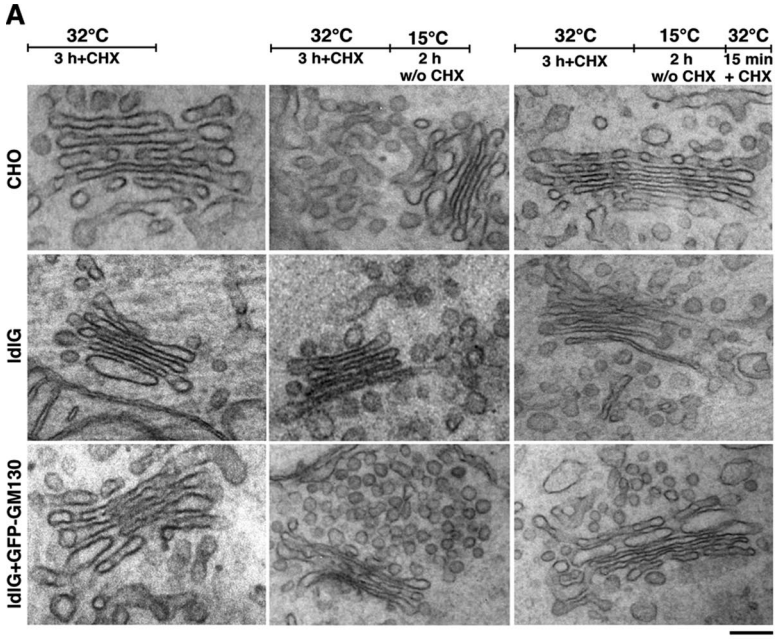

B

	Cisternae			EGCs			Vesicles+Tubules			n° Cisternae/Stack		
	CHO	ldlG	ldlG+ GM130	CHO	ldlG	ldlG+ GM130	CHO	ldlG	ldlG+ GM130	CHO	ldlG	ldlG+ GM130
32°C 3 h+CHX	**32.03** (±10.7)	**17.09** (±5.9)	**26.26** (±7.8)	**6.10** (±6.0)	**4.18** (±4.0)	**14.11** (±10.4)	**5.22** (±3.1)	**6.59** (±3.1)	**6.21** (±3.2)	**5.24** (±1.0)	**3.56** (±0.9)	**4.36** (±1.0)
32°C 15°C 2 h w/o CHX 3 h+CHX	**22.55** (±7.0)	**17.31** (±5.0)	**16.44** (±5.9)	**29.74** (±14.6)	**14.22** (±8.0)	**35.63** (±21.7)	**8.35** (±3.7)	**5.03** (±2.6)	**3.85** (±2.3)	**4.18** (±0.9)	**3.64** (±0.9)	**3.83** (±0.9)
32°C 15°C 32°C 2 h 15 min w/o CHX + CHX 3 h+CHX	**51.73** (±11.6)	**23.74** (±9.0)	**37.70** (±13.3)	**4.87** (±5.5)	**10.71** (±9.2)	**14.37** (±8.7)	**18.66** (±4.8)	**6.32** (±3.1)	**8.41** (±3.4)	**5.28** (±1.9)	**4.20** (±0.9)	**4.72** (±0.7)

Figure 2. GM130 mediates incorporation of EGCs into the Golgi cisternae. (A) VSV-infected CHO, ldlG cells, and ldlG cells transfected with GFP-GM130 (as indicated) were treated with CHX and NZ for 3 h at 32°C (steady state) and then shifted to 15°C for 2 h without (w/o) CHX, followed by 15 min at 32°C with CHX. Representative EM images of Golgi stacks and EGCs are shown. Bar, 120 nm. (B) Morphometric analyses of the EGCs and GC under the treatments shown in A (see *Materials and Methods*).

most, highly perforated Golgi cisterna appeared (data not shown). Thus, in CHO cells, the incoming EGC membranes are completely redistributed into the Golgi stacks, in part to build up the *cis*-most, highly perforated cisterna and in part to enlarge all of the preexisting cisternal plates (see also Trucco *et al.*, 2004).

In comparison to the CHO cells, the ldlG cells showed several significant differences (Figure 2): in the ldlG cells, the ratio between Golgi cisternae and tubulovesicular peri-Golgi elements at steady-state was lower (1.33 in ldlG cells vs. 2.8 in CHO cells) and at 15°C, the changes in surface area of the Golgi stacks and the EGCs were smaller than in the CHO cells. The most remarkable differences were seen, however, after the resumption of transport upon release of the temperature block, when 1) the surface area of the EGCs decreased by only ~25% in the ldlG cells, compared with by almost 85% in the CHO cells; 2) the surface area of the cisternae increased by only ~35% in the ldlG cells, but it more than doubled in the CHO cells; and 3) the number of cisternae per stack did not significantly change in the ldlG cells, compared with the statistically significant increase seen for the CHO cells. Interestingly, with the expression of full-length GM130 in the ldlG cells, the difference seen between CHO cells and ldlG cells in the efficiency of incorporation of EGCs into the stacks was strongly attenuated (in terms of surface area) and even abrogated (in terms of the number of cisternae), directly demonstrating that the defects observed in ldlG cells were specifically due to the absence of GM130 (Figure 2).

Formation and Maintenance of the Golgi Ribbon Requires GM130-mediated Incorporation of EGCs into the Stacks

Our findings show that input of EGC membranes is required for the formation and maintenance of the Golgi ribbon and that GM130 is needed for the incorporation of EGCs into the GC, at least in this simplified ministack system. This prompted us to investigate the role of GM130 in the structural organization of the Golgi ribbon in cells with an intact microtubule system.

As detailed in the Supplementary Material (Supplementary Figure S1), a combination of four independent approaches was used to knock out GM130. These included: 1) injection of an antibody against the 309 N-terminal amino acids of hGM130 (N309), which induces a complete and proteasome-dependent degradation of endogenous GM130 in <3 h; 2) overexpression of a truncated form of GM130 that is devoid of the 300 N-terminal amino acids (G95; Fritzler *et al.*, 1993; Marra *et al.*, 2001), which induces the disappearance of endogenous full-length GM130 within 16 h; 3) treatment

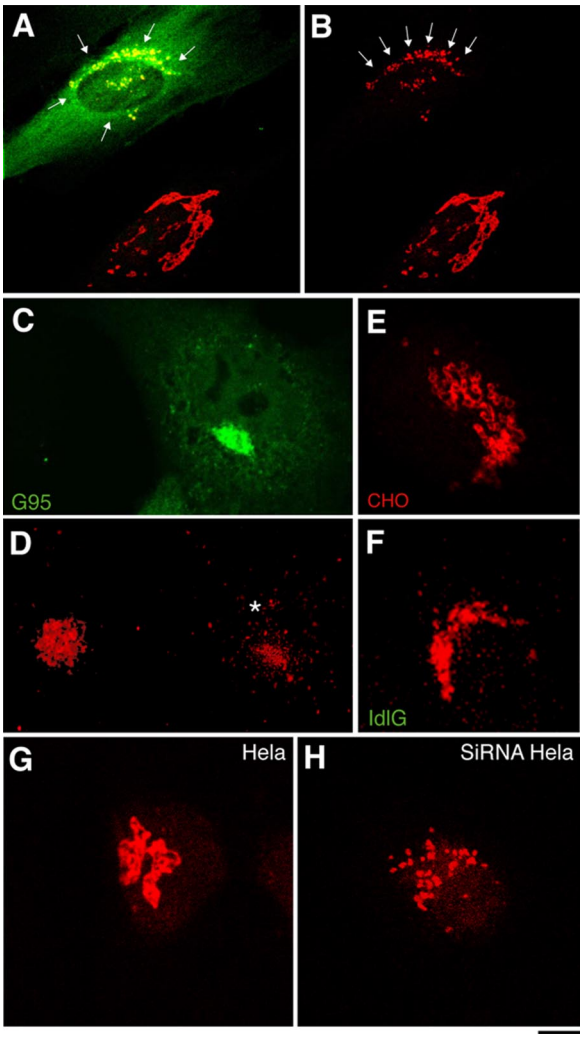

Figure 3. The Golgi ribbon is fragmented in GM130-depleted cells. (A and B) HFs were injected with the N309 anti-GM130 antibody and after 1 h at 37°C they were fixed and stained for N309 (A; green) and giantin (A and B; red). In noninjected cells (lower right), giantin staining is reticular and continuous; in N309-injected cells (top left) it shows discrete small puncta (A and B, arrows). (C and D) COS7 cells were transfected with GFP-G95, and 20 h later (when no endogenous GM130 was detectable; Supplementary Figure S1) they were fixed; GFP-G95 fluorescence (C; green) and giantin staining (D; red) are shown. Note that the staining pattern for giantin is disorganized in transfected cells (D, asterisk; right) compared with nontransfected cells (D, left). (E and F) CHO (E) and ldlG cells (F) were stained for giantin (red). Note that the regular pattern of interconnected ring-like structures in CHO cells is absent in ldlG cells, which show small solid dispersed puncta. (G and H) Hela cells were mock-treated (G) or treated with siRNAs for GM130 (72 h; H) and fixed and stained for giantin (red). Bar, 3 μm (A, B, E, and F); 10 μm (C and D); 2 μm (G and H).

with hGM130 siRNAs for 48–96 h; and 4) use of the previously described ldlG cells.

The acute knockout of GM130 through injection of N309 in HFs (and in COS7, HeLa, NRK, and A375 cells) changed the staining pattern of the Golgi marker giantin from that of the regular continuous structures of the control cells into an irregular clustering of spots that were located in the pericentriolar area (Figure 3, A and B). An analogous difference in the staining patterns of giantin emerged from a comparison of control COS7 cells with COS7 cells depleted of their endogenous GM130 through the overexpression of G95 (Figure 3, C and D), of CHO cells with ldlG cells (Figure 3, E and F), and of control HeLa cells with HeLa cells treated with GM130-directed siRNAs (Figure 3, G and H).

Of note, under all of these circumstances, the changes in the organization of the GC induced by the absence of GM130 were accompanied by changes in the distribution of proteins cycling between the ER and the GC, including the KDEL receptor (KDELR; Figure 4), p23, ERGIC53, and Rab1 (not shown). Indeed, while these proteins were localized both in the central Golgi area and in peripheral structures in control cells, they underwent massive peripheral redistribution in the absence of GM130, confirming that the incorporation of incoming membranes into the GC is impaired in the absence of GM130.

The ultrastructure of the GC was then examined in cells injected with the N309 antibody. Golgi stacks of very variable sizes were seen in mock-injected cells (from 350 to almost 7000 nm in HFs), as expected from the random sectioning of a ribbon-like structure (Figure 5, A and B). In contrast, only isolated stacks of more homogeneous and smaller sizes were seen in the pericentriolar area of N309-injected cells (ranging from 270 to 1400 nm in HFs), where a higher number of vesicular and tubular structures were also seen surrounding the stacks (Figure 5, A and B). A very similar pattern of fragmentation of the GC was seen in COS7 cells lacking endogenous GM130 due to the overexpression of G95; here, the Golgi ribbon was also absent, and it was replaced by isolated stacks with irregular cisternae and with vesicles, tubules, and pleiomorphic structures (Figure 5C).

We then performed a comparative analysis of the ultrastructure of the GC in the COS7 and ldlG cells at the permissive temperature. At a first level of analysis, the EM revealed the presence of stacks of cisternae comparable to the parental CHO cells (see Vasile *et al.*, 2003). However, an analysis of thin serial sections showed that although in CHO cells the length of the cisternae can vary (from 300 to 2000 nm) as a result of random sectioning of a ribbon-like structure, in ldlG cells, this length was almost invariably ~500 nm, as expected from the random sectioning across isolated stacks (Figure 5, D, E, and H). These results from serial-section reconstructions were confirmed by the electron-tomography analysis, which showed that as opposed to the ribbon-like structure of the CHO cells, the isolated stacks in ldlG cells never formed such a structure (Figure 5, F and G). In addition, a greater number of pleiomorphic structures were seen to accumulate around the stacks in ldlG cells, including vesicles, tubules, and convoluted structures (Figure 5). Importantly, the lengths of the cisternae and their length variability increased in ldlG cells upon transfection with GM130 (Figure 5H).

Finally, to provide independent evidence of the discontinuity of the Golgi ribbon in cells depleted of GM130, the kinetics of the Golgi enzymes were analyzed. Although in CHO cells the Golgi enzymes freely diffused along the ribbon (as evaluated by fluorescence recovery after photobleaching, and as described by Cole *et al.* (1996), in ldlG cells they appeared to be segregated within the isolated stacks (Supplementary Movies 1 and 2). This thus confirmed that the absence of GM130 is accompanied by the loss of continuity of the Golgi ribbon.

Altogether, these results demonstrate that by mediating this fast and complete incorporation of EGCs into the stacks, GM130 regulates the balance between cisternal and tubulovesicular membranes in the stacks and ensures the continuity of the Golgi ribbon.

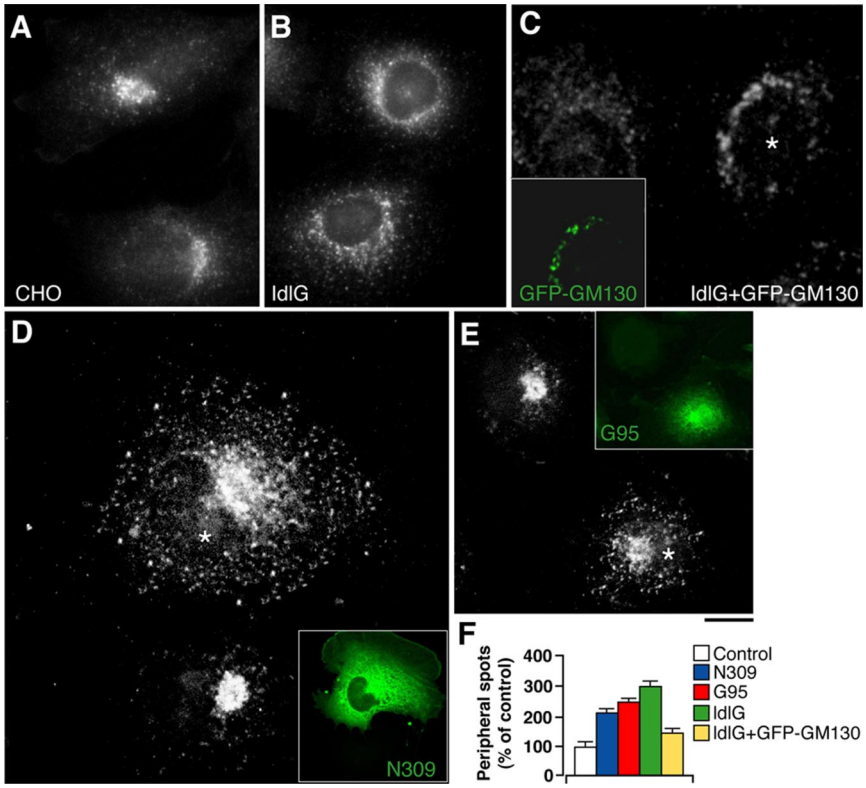

Figure 4. ER-to-Golgi recycling proteins accumulate in EGCs in the absence of GM130. CHO (A), ldlG cells (B), and ldlG cells transfected with GFP-GM130 (C) were fixed and stained for the KDELR. Note that the KDELR is present mainly in peripheral punctate structures in ldlG cells, whereas it is also on the central GC in CHO cells and in ldlG cells transfected with GFP-GM130 (C, asterisk). Inset, GFP-GM130 staining of the transfected cell in (C) (green). (D) COS7 cells were injected with the N309 antibody (asterisk) and stained for the KDELR. Note that the KDELR is redistributed to the periphery in the N309-injected cell, compared with a noninjected cell (top left). Inset, N309 staining of the transfected cell in D (green). (E) COS7 cells were transfected with G95 and stained for the KDELR. Note the peripheral redistribution of the KDELR in a G95-overexpressing cell (asterisk), compared with a nontransfected cell (bottom). Inset, GFP-G95 staining of the transfected cell in E (green). Bar, 8 μm (A, B, and E); 5 μm (C and D); 7.5 μm (inset in C and E); 16 μm (inset in D). (F) Quantitation of the peripheral redistribution of the KDELR. The ratios between fluorescence of peripheral puncta and pericentriolar Golgi structures are expressed as percentages of the relative control cells (untreated or mock-injected COS7 cells for G95-expressing cells; N309-injected COS7 cells and CHO cells for ldlG cells; and ldlG cells transfected with GFP-GM130).

GM130 Mediates the Structural Maturation and Coalescence of EGCs

The ability of GM130 to continuously cycle between the *cis*-Golgi compartments and the subpopulation of EGCs that represent be the next to be delivered to the GC (Marra *et al.*, 2001) suggested that GM130 might directly control some of the properties of the EGCs, such as their dynamics, structure, and composition, which could be instrumental in their entry/incorporation into the Golgi stacks.

Indeed, GM130-positive EGCs showed distinctive features. First, the vast majority of GM130-positive EGCs were larger than 400 nm, whereas only some 5% of the GM130-negative carriers were of comparable size. Second, although the GM130-negative EGCs appeared mainly as tubulovesicular structures, the GM130-positive EGCs mostly consisted of tubules organized into bundles and of flat discs decorated with coated buds (if they also contained COPI); these latter also appeared as complex structures made up of two or three associated discs (Figure 6, A–P). Thus, the presence of GM130 on the EGCs correlated with the presence of multiple, closely juxtaposed structures, suggesting a role for GM130 in mediating their tethering.

When monitored in living cells, EGCs showed intense motility and underwent several and repetitive "coalescence events" (defined as those events in which two distinct EGCs merged into one and from that time on move as a single entity; Figure 7A and Supplementary Movie 3). These events occurred much more frequently between two GM130-positive EGCs than between two GM130-negative ones or between one GM130-negative and one GM130-positive EGC (Figure 7B). Coalescence between two EGCs might be considered as a preliminary step in the formation of larger structures, possibly through homotypic fusion. Consistent with this possibility, inhibiting SNARE-mediated fusion with the L294A αSNAP mutant (Barnard *et al.*, 1997) resulted in an increase in the number and a decrease in the size of GM130-positive EGCs (Figure 7, C–E). It also caused an increase in the number of nonproductive coalescence events, which were defined as those events in which two EGCs apparently converged and coalesced, but then rapidly diverged and moved away separately to different destinations (Figure 7, E and F, and Supplementary Movie 4).

To determine whether GM130 has a role in the tethering between EGCs that may precede their fusion, the impact of knocking out GM130 on the dynamics and size of EGCs was also evaluated. In the absence of full-length GM130, EGCs were more numerous (Figure 7, C and D) and smaller, and underwent coalescence with half the frequency seen under control conditions (Figure 7F). These results indicate that GM130 is required for the homotypic tethering of EGCs that preludes their transition into the more homogenous, larger, and mature carriers that are ready to be incorporated into the GC.

The Absence of GM130 Causes a Kinetic Delay in the Arrival of Cargo at the GC, But No Defects in its Glycosylation

The above data indicated that GM130 has an essential role in mediating the fast and complete incorporation of EGCs into the Golgi stacks and that this incorporation is required for assuring the continuity of the Golgi ribbon. The next question was whether EGCs need to be completely integrated into the stacks (i.e., need GM130) to deliver secretory cargo to the GC.

To this end, the transport of the reporter protein VSVG was probed in control and GM130-depleted cells, using VSV-infected, N309-injected HFs and COS7 cells. In both cell types, VSVG accumulated in the ER at 40°C, and 5 min after release of the temperature block it was present in peripheral spots, i.e., EGCs. However, at 15 min, when almost all of the

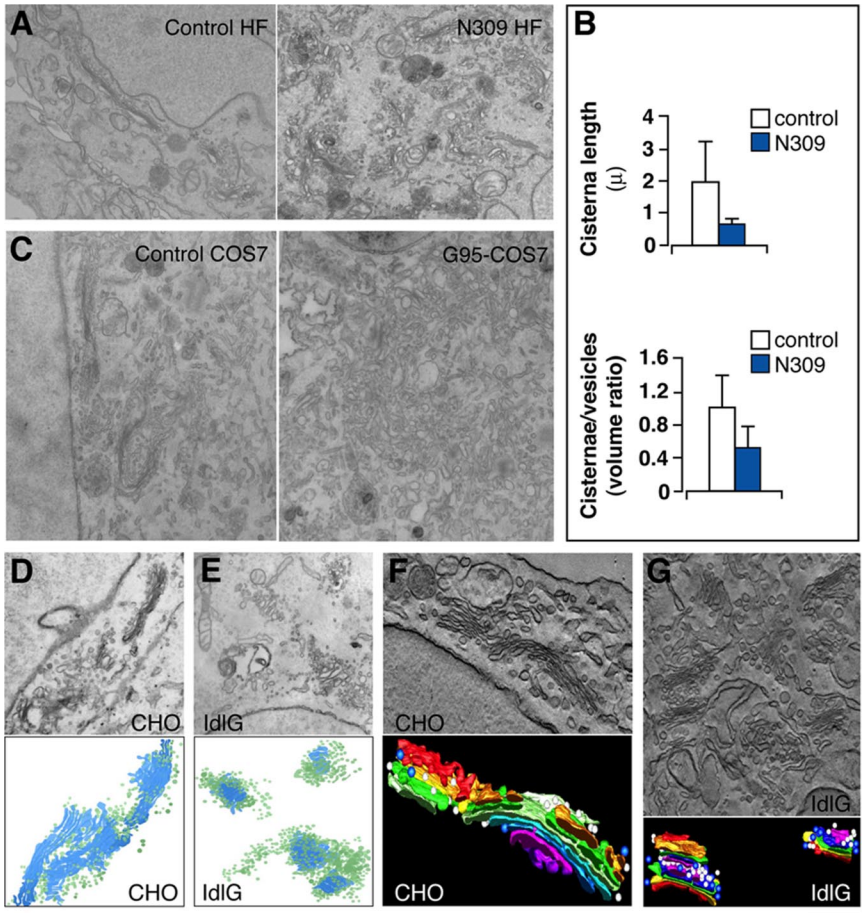

H

	CHO	IdlG	IdlG+GM130
Cisterna length (nm±SD)	733±346	510±192	714±213
Stack coalescence (number/stack)	0.36	0.06	ND
Round profiles/cisternae (surface area)	0.3	0.7	ND

Figure 5. GM130 depletion induces fragmentation of the Golgi ribbon, shortening of the cisternae, and accumulation of tubulovesicular membranes. Control and N309-injected HFs (A and B), and control and G95-overexpressing COS7 cells (C) were processed for EM (A and C) and morphometric analysis (B), as described in *Materials and Methods*. CHO and ldlG cells (D–G) were analyzed by EM serial sectioning (D and E) or EM tomography (F and G). Bottom panels in D and E show superimposition of Golgi (blue) and tubule and vesicle (green) profiles in six consecutive serial sections. Bottom panels in F and G show 3D EM-tomography reconstructions, with *cis*-most (red) and *trans*-most (magenta) cisternae. Vesicles (blue, 50–60 nm; white, 80–90 nm) are represented by software-generated spheres, centered on the center of the vesicles. Bar, 1 μm (A and C–E); 600 nm (F and G). (H) Morphometric analysis of the Golgi area in serial sections from CHO cells, ldlG cells, and ldlG cells expressing GFP-GM130 (see *Materials and Methods*). Stack coalescence is where two apparently distinct stacks on one section become one stack on the next section. The number of these coalescence events is related to the number of stacks in the sections.

VSVG was associated with pericentriolar Golgi structures in control cells, in the N309-injected cells, a significant fraction of the VSVG was still in peripheral carriers (Figure 8, A and D), indicating a delay in its delivery into the central GC. Similarly, 30 and 45 min after release of the temperature block, the arrival of VSVG at the plasma membrane was delayed in N309-injected cells, compared with control cells, although it reached levels indistinguishable from control cells at later times (60 min; Figure 8B). A delay in ER-to-Golgi transport of VSVG was also seen in cells depleted of endogenous GM130 by the overexpression of G95 (Figure 8D).

The transport of VSVG was also monitored in ldlG cells. Given the temperature sensitivity of this cell line (nonpermissive for ldlG at 39.5°C), an adapted synchronization protocol was used to follow ER-to-Golgi transport of VSVG at the permissive temperature of 32°C (see *Materials and Methods*). Under these conditions, transport of VSVG from the ER to the GC was slower in ldlG cells, compared with CHO cells: when VSVG reached the late compartments of the GC (i.e., the *trans*-Golgi network) in CHO cells, it was still at the level of the peripheral EGCs in ldlG cells (Figure 8, C and D). Also in this case, the lack of GM130 and of a Golgi ribbon only resulted in a delay in the transport of this secretory cargo, because at later time points the amount of VSVG transported into and out of the GC was indistinguishable in CHO and ldlG cells.

These results demonstrate that the delivery of ER-derived secretory cargo to the GC and its progression through and out of the GC can occur in the absence of GM130, albeit with a lower efficiency. Thus the complete incorporation of EGCs into the stacks appears not to be absolutely required for anterograde progression of cargo, for which even limited and/or transient connections between EGCs and the GC might be sufficient.

Our observations here that the absence of GM130 interrupts the continuity of the Golgi ribbon and impairs the lateral diffusion of Golgi glycosylating enzymes while having only marginal effects on the progression of secretory cargo, prompted us to investigate whether GM130 could affect the efficiency/completeness of glycosylation of neo-

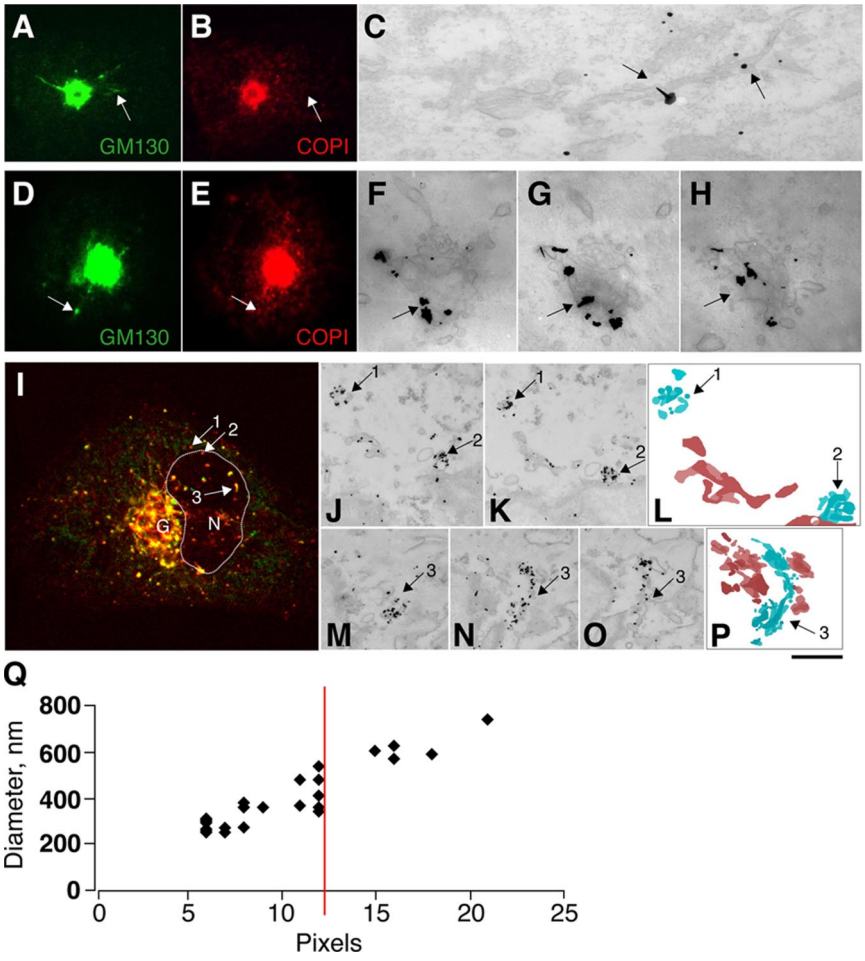

Figure 6. GM130-positive EGCs are larger and have a more complex structures than GM130-negative EGCs. (A–H) COS7 cells at steady state were stained for GM130 (A and D; green) and COPI (B and E; red) and processed for CLEM (C and F–H; see *Materials and Methods*). EGCs containing either GM130 alone (A–C, arrows) or both GM130 and COPI (D–H, arrows) were examined for GM130 after immuno-EM labeling and nano-gold-enhancement (F–H are 50-nm-thick consecutive tangential serial sections). (I–P) COS7 cells were infected with VSV and placed at 40°C for 3 h. The cells were then shifted to 32°C for 15 min and stained (I) for VSVG (red) and GM130 (green) and processed for CLEM (J–P; see *Materials and Methods*). In I, G indicates the Golgi area; N and the delineated area indicate the nucleus. VSVG was further labeled by nano-gold-enhancement in consecutive serial sections (J, K, and M–O). Numbered arrows (I–P) show corresponding GM130-negative (arrows 1 and 2) and GM130-positive (arrow 3) EGCs. Superimposition of consecutive serial sections showing GM130 negative (L) and GM130 positive (P) EGCs (blue) and ER (brown). Bars, 10 μm (A, B, D, and E); 3 μm (I); 200 nm (C and F–H); 500 nm (J, K, and M–O); and 700 nm (L and P). (Q) Correlation between the diameters of the EGCs at the immunofluorescence and EM levels (see *Materials and Methods*). Note that more than 90% of the GM130-positive EGCs were of a size that was at least in one dimension greater than 12 pixels (corresponding to 450 $\pm$ 150 nm), whereas the vast majority (80%) of GM130-negative EGCs were smaller (data not shown).

synthesized secretory cargo. While this article was in preparation, a similar hypothesis was proposed by Puthenveedu *et al.* (2006) based on their studies in cells treated with siRNAs for GM130. We took different approaches to address this issue, by comparing the glycosylation of neosynthesized exogenous and endogenous proteins in cells with and without GM130 and thus with and without an intact Golgi ribbon.

We first compared the ldlG and CHO cells at the permissive temperature (32°C; see above). At this temperature, we could see no significant differences in the processing and transport of LDLR between CHO and ldlG cells (Figure 8E), in agreement with Hobbie *et al.* (1994), who reported normal posttranslational processing of membrane-associated proteins (including ldl receptor [ldlR]) and secretory proteins in ldlG cells at the permissive temperature (Hobbie *et al.*, 1994), as opposed to the block of processing and secretion observed at the nonpermissive temperature (39.5°C).

We also assessed the efficiency and extent of glycosylation of VSVG protein by measuring the acquisition of Endo-H resistance (as an index of mannosidase II [ManII] activity) and neuraminidase sensitivity (as an index of sialyltransferase activity) of the neosynthesized protein. As illustrated in Figure 8F, ldlG cells showed an altered pattern of glycosylation of VSVG compared with CHO cells at the permissive temperature. This was seen at all of the chase times, including the very late ones (60 min), as a band of a lower molecular weight compared with that in CHO cells (Figure 8F). Of note, this nonmature form was transported to the plasma membrane in ldlG cells, as revealed by cell-surface biotinylation. In the first instance, this finding favored the hypothesis that the presence of a continuous Golgi ribbon is required to control the efficiency of glycosylation. To further test this hypothesis, three approaches were taken: 1) exogenous transfection of GM130 in ldlG cells, a process that restores the continuity of the Golgi ribbon, to determine whether this restored the "normal" pattern of VSVG glycosylation (Figure 8F); 2) assessment of the glycosylation patterns of VSVG and endogenous proteins in cells in which the expression of GM130 had been silenced by independent means (transfection of G95 or with siRNAs, where the Golgi ribbon was fragmented; Figure 8G); and 3) assessment of the glycosylation patterns of VSVG in CHO cells in which the Golgi ribbon had been fragmented by GM130-independent means (microtubule depolymerization with NZ; Figure 8H). Neither the stable expression of GM130 in ldlG cells (under conditions in which it restored the continuity of the Golgi ribbon) had detectable effects on the glycosylation defect in ldlG cells (Figure 8F), nor was a similar defect detected in G95 overexpressing cells or in cells treated with the GM130 siRNAs (Figure 8G). Finally, the fragmentation of the Golgi ribbon into ministacks induced by nocodazole also did not induce any glycosylation defect in CHO cells (or in NRK and COS7 cells, and HFs) and did not affect the defect in ldlG cells (Figure 8H). Thus the abnormal glycosylation pattern of VSVG seen in ldlG cells at the permissive temperature cannot be ascribed to the lack of GM130 or the Golgi ribbon;

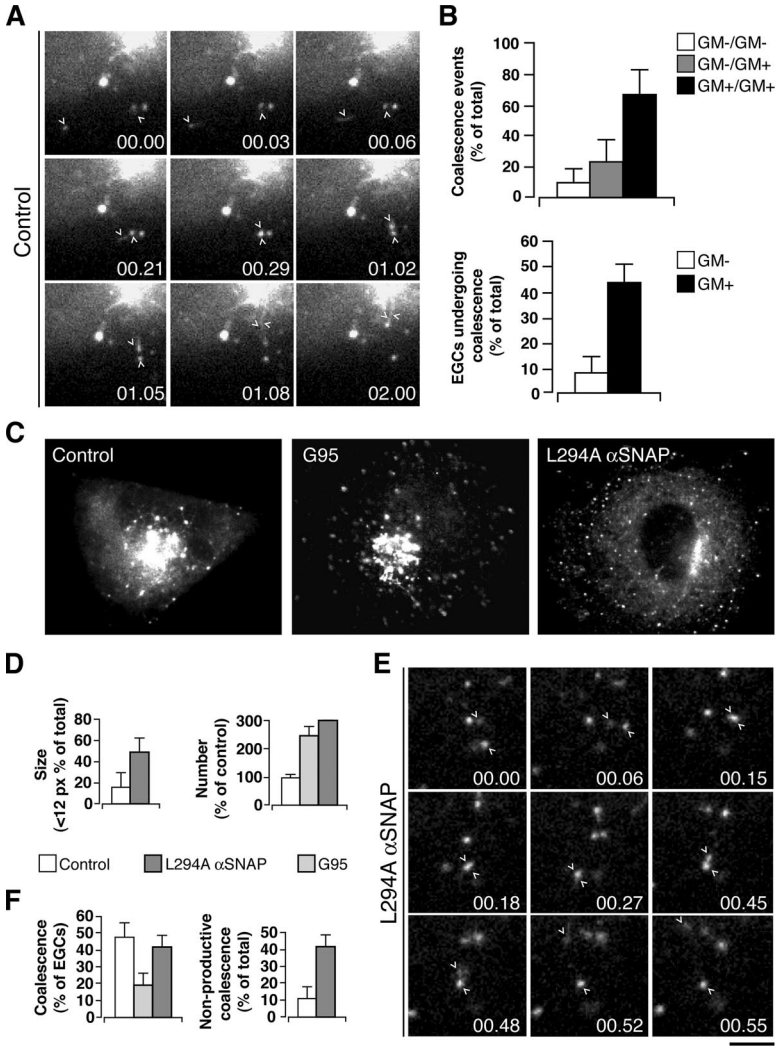

Figure 7. Dynamics of GM130-positive EGCs in COS7 cells. (A) Peripheral motile structures in cells expressing GFP-GM130 (control) were imaged under time-lapse microscopy. Selected frames shown at the indicated times; arrowheads indicate structures that coalesce (00.03–00.29) and then move together (01.02–01.08) until they are no longer resolvable (02.00). (B) Quantitation of coalescence events attributable to GM130-positive (GM+) and GM130-negative (GM−) EGCs and of EGCs of each category exhibiting coalescence events. Cells were cotransfected with VSV-YFP and CFP-GM130, kept at 40°C for 12 h, then shifted to 32°C, and after 5 min imaged under time-lapse microscopy. (C–F) GFP-GM130–expressing cells (Control), GFP-G95–overexpressing cells (G95), and GFP-GM130–expressing cells injected with the mutant αSNAP L294A were fixed (C and D) or imaged under time-lapse microscopy (E and F). (D) Quantitation for size and number of GM130-positive EGCs as shown in c (as indicated). (E) Nonproductive coalescence events of EGCs in cells expressing GFP-GM130 and injected with αSNAP L294A under time-lapse microscopy. Two EGCs (arrowheads) apparently converge and coalesce (00.006–00.27), then rapidly diverge (00.45, 00.48) and move separately to different destinations (00.52, 00.55). (F) Quantitation of the total coalescence events and nonproductive coalescence events as shown in C and E (as indicated). Bar, 3 μm (A and E), 10 μm (C).

rather, it might be linked to unrelated and pleiotropic defects present in this cell line (Vasile *et al.*, 2003).

To detect possible glycosylation defects of endogenous cargo, we also assessed the glycosylation of the HCAM cell adhesion molecule (Figure 8I) and compared the general lectin-staining pattern of cells with or without GM130 and/or with or without an intact Golgi ribbon; this latter approach used lectins that specifically recognize terminal sialic acid (SNAI) or terminal *N*-acetyl-D-glucosamine (GSII). As before, this approach did not reveal any notable differences between and among these cells (Figure 8J).

Altogether these results did not allow any correlation to be established between the fidelity and efficiency of the glycosylation process and the presence of an intact Golgi ribbon and/or of GM130.

DISCUSSION

The GC is a key station along the secretory pathway in all eukaryotic cells, where highly conserved functions are performed, including glycosylation and the transport and sorting of neosynthesized proteins and lipids. However, the GC is present in different organisms in very different forms: from scattered tubulovesicular structures (*Saccharomyces cerevisiae*), via isolated multiple stacks of cisternae (*Pichia pastoris*, *Drosophila*, and plants), to a continuous pericentrosomal ribbon that is made up of interconnected stacks of flat cisternae (mammals). The reasons for such a variegate architecture of this organelle in different organisms despite its very "conserved" functions are not yet really understood.

We show here that the continuous ribbon configuration of the GC in mammalian cells reveals the "active" state of the organelle, as it receives and incorporates membranous carriers from the ER (i.e., the EGCs); this is illustrated figuratively in Figure 9. However, as soon as this input of membranes from the ER is slowed down or interrupted, this ribbon undergoes disconnection into isolated Golgi stacks with shorter cisternae (see Figure 9). This thus provides a further example of the high degree of plasticity of the GC, which undergoes an extensive remodeling that is dependent on its level of activity and the developmental stage of the cell (Jasmin *et al.*, 1989; Clermont *et al.*, 1993; Marsh *et al.*, 2004; Trucco *et al.*, 2004).

This arrival of ER-derived membranes is necessary but not sufficient per se to sustain the formation of the Golgi ribbon, as we have shown here that a further requirement is the complete incorporation/integration of these membranes into the cisternal stacks. This process implies the transition of highly pleiomorphic membranes (i.e., the EGCs; Klumperman, 2000) into regular flat discs (i.e., the Golgi cisternae), and it requires the

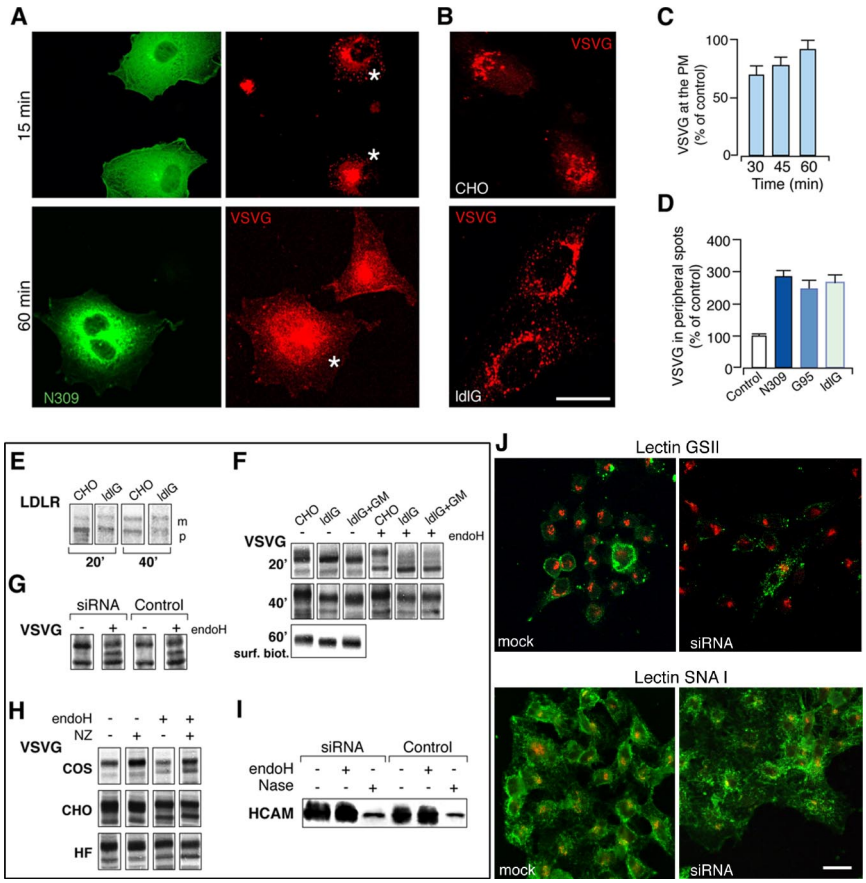

Figure 8. The absence of GM130 causes a kinetic delay in the arrival of cargo at the Golgi complex, but no defects in its glycosylation. (A) VSV-infected COS7 cells were injected with a control antibody or the N309 antibody, incubated at 40°C for 2 h, shifted to 32°C for the indicated times, and then stained for N309 (green) and VSVG (red). After 15 min, VSVG is mainly localized in the GC in mock-injected cells, whereas it is still in peripheral structures in N309-injected cells (top panels, asterisks). After 60 min, VSVG reaches the plasma membrane in both mock-injected and N309-injected cells (bottom panels, asterisk). (B) CHO and ldlG cells were infected with VSV and incubated at 32°C in the presence of CHX for 3 h. After CHX washout, the cells were shifted to 15°C for 2 h to allow VSVG to accumulate in the intermediate compartment and then incubated again at 32°C for 15 min in the presence of CHX. The cells were fixed and stained for VSVG, which is seen to be in the GC in CHO cells, and retained in peripheral structures in ldlG cells. Bar, 10 μm (A); 5 μm (C). (C) Quantification of VSVG transported to the plasma membrane was calculated as the ratio between VSVG at the plasma membrane (labeled with an anti-luminal VSVG antibody in nonpermeabilized cells) and total VSVG (GFP labeled). The VSVG transport in N309-injected cells transfected with GFP-VSVG is shown as a percentage of that in mock-injected cells. (D) Quantification of ER-to-Golgi transport of VSVG as shown in (C). This was calculated as the ratio between VSVG staining in peripheral structures and in the GC in cells depleted of GM130 (by N309 injection or G95 expression, or in ldlG cells; as indicated), with respect to the relevant control cells (COS7 cells for N309-injected and G95-expressing COS7 cells; CHO cells for ldlG cells). (E–J) Analysis of posttranslational processing of exogenous and endogenous secretory proteins in cells with and without GM130 and with or without an intact Golgi ribbon. (E) The posttranslational modification of LDLR was assessed in GFP-LDLR transfected CHO and ldlG cells. After pulse with [^{35}S]methionine and 20 and 40 min of chase, cells were lysed and cell lysates immunoprecipitated with anti-GFP antibodies; m, mature; p, precursor forms of GFP-LDLR. (F) The glycosylation of neosynthesized VSVG was analyzed with pulse-chase experiments and Endo-H treatment in CHO and ldlG cells and in ldlG cells expressing GFP-GM130 (ldlG+GM). After 20 and 40 min of chase, the cells were lysed, and the total [^{35}S]-labeled VSVG was analyzed by SDS-PAGE without and with Endo-H treatment (as indicated). After 60 min of chase, the fraction of VSVG transported to the plasma membrane was measured by cell surface biotinylation. VSVG appears as a lower molecular weight band in ldlG cells and in ldlG cells transfected with GFP-GM130, compared with CHO cells, at all times of the chase, and it is transported as such to the cell surface. Also, in ldlG cells, compared with CHO cells, there is a delay in acquisition of Endo-H resistance seen at 20 min that is recovered by 40 min. (G) The glycosylation of VSVG was analyzed with pulse-chase experiments in mock-treated HeLa cells (Control) or HeLa cells treated for 78 h with siRNAs against GM130. After 60 min of chase, no substantial differences were seen between control and GM130-depleted cells. (H) The glycosylation of neosynthesized VSVG was analyzed by treatment with Endo-H in control cells (COS7 and CHO, and HFs) or after fragmentation of the Golgi ribbon with NZ (as indicated). No differences in the glycosylation patterns of VSVG were seen between control and treated cells. (I) The glycosylation pattern of the endogenous HCAM glycoprotein was assessed by treating cell lysates (from mock-treated or GM130-siRNAs-treated HeLa cells) with Endo-H or neuraminidase (Nase). Both in control and GM130-depleted cells, HCAM is properly sialylated at steady state (as indicated by the shift of the band upon treatment with Nase). (J) Mock-treated or GM130-siRNA–treated HeLa cells (72 h) were stained with Alexa fluor 488-lectin GSII (specific for terminal *N*-acetyl-D-glucosamine; green) or fluorescein-lectin SNAI (specific for sialic acid; green; as indicated), and with giantin (red). No significant differences were seen between control and GM130-depleted cells, with ≥97% of cells showing plasma-membrane positivity for SNA lectin and ≤3% showing plasma-membrane positivity for GSII (see *Materials and Methods*). Bar, 15 μm.

Golgi matrix protein GM130. Indeed, we have previously shown that EGCs acquire GM130 during the late stages of their transport to the GC (Marra *et al.*, 2001), and here we show that through this acquisition of GM130, they develop the ability to undergo homotypic coalescence and fusion. The direct consequence is that the EGCs become larger in size and more homogenous in shape (i.e., disk-like shapes; Figure 9). These kinetic and structural changes induced by GM130 can thus be viewed as a sort of maturation process through which the EGCs acquire properties and composition closer to those of the next compartment, i.e., the Golgi cisternae. Indeed, the arrival of a synchronized population of EGCs at the GC coincides with an immediate increase in both the number of cisternae per stack and the surface area of the cisternae (concomitant with a decrease in the surface area of the EGCs), thus indicating the complete transition/incorporation of the EGCs into the cisternae. This transition requires GM130 because in its absence (induced here by four independent approaches) the incorporation of the pleiomorphic EGCs into the Golgi stacks is impaired and the EGCs remain as distinct entities, with the result that: 1) tubulovesicular membranes accumulate; 2) the highly fenestrated *cis*-most cisterna (of which the EGCs might be considered as the immediate precursors) disappears; 3) the length of the

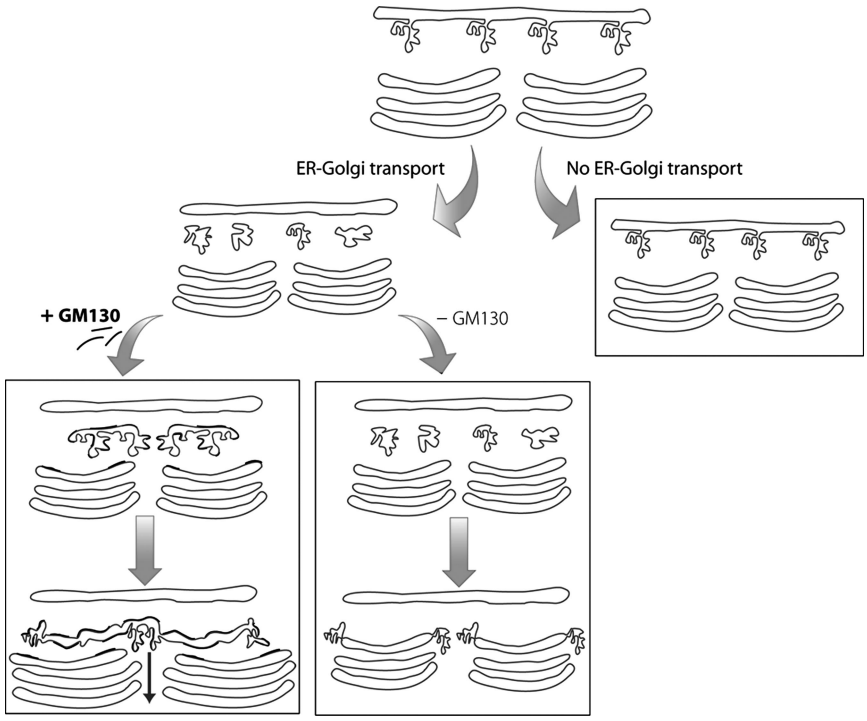

Figure 9. Model of the roles of membrane input from the ER and of GM130 in the biogenesis of the Golgi ribbon. In the absence of membrane input from the ER (no ER-to-Golgi transport) the Golgi ribbon undergoes disconnection into isolated stacks, the *cis*-fenestrated cisterna disappears and the overall length of the cisternae decreases. In the presence of membrane input from the ER (ER-to-Golgi transport) the ER-to-Golgi carriers (EGCs) are transported to the GC: if they acquire GM130 (+GM130), they undergo homotypic coalescence-fusion generating larger and more homogenous disk-like membranes that are directly incorporated into the stacks, contributing to a new fenestrated cisterna at the *cis* pole and participating in the formation of the ribbon. In the absence of GM130 (−GM130), the incorporation of the EGCs into the stacks is impaired and they remain as distinct entities that are however still able to deliver cargo through limited continuities with the GC. This causes the accumulation of tubulovesicular membranes, the disappearance of the highly fenestrated *cis*-most cisterna, the overall shortening of the cisternae and the disconnection of the Golgi ribbon.

cisternae decreases; and 4) the continuity of the Golgi ribbon is interrupted (Figure 9). However, although remaining as apparently distinct entities, these carriers still appear to be able to establish continuities, either limited and/or transient, with the different Golgi compartments, as witnessed by the fact that secretory cargo can still be delivered to the GC in the absence of GM130, although with a lower efficiency (Figure 9).

Thus, the GM130-positive EGCs (defined as L-IC in Marra *et al.*, 2001) identifies the compartment in the mammal secretory pathway where the transition from dissociative and isolated pre-Golgi membranes (i.e., the EGCs) to the continuous Golgi membrane system (i.e., the cisternae in the ribbon) occurs (Figure 9). In fact the observation that the GM130-centered machinery, a machinery operating at the entry point of the Golgi stacks, is able to condition the organization of the entire Golgi ribbon is consistent with the cisternal maturation view according to which the late Golgi compartments evolve from earlier ones (Mironov *et al.*, 2001; Losev *et al.*, 2006; Matsuura-Tokita *et al.*, 2006).

While this manuscript was in preparation, it was reported that in HeLa cells treated with GM130-targeted siRNAs, the GC is fragmented (Puthenveedu *et al.*, 2006). Thus our results are in agreement with this observation, although here we propose a different mechanism of action for GM130. Indeed, Puthenveedu *et al.* (2006) proposed that the activity of GM130 in the formation of the Golgi ribbon is not in mediating the tethering of vesicular membranes, but rather in mediating the homotypic fusion of neighboring cisternae, also because they could not measure an increase in the number of vesicles in cells treated with GM130-targeted siRNAs. By performing a morphometric analysis in cells depleted of GM130 by four independent means, we show here that in the absence of GM130 there is actually an accumulation of tubulovesicular membranes (as compared with cisternal membranes). We believe that the explanation for the discrepancy between these two sets of data are to be found in the differences in the experimental approaches used and in the different criteria used to measure the tubulovesicular membranes: a morphometric measure of the ratio of tubulovesicular membranes to cisternal membranes in the Golgi area under four independent conditions of GM130 knockout in different cell types (the present study), compared with an assessment of the absolute number of vesicles or the isolation of a selected population of vesicles containing the recycling protein Gpp130 in HeLa cells treated with siRNAs for GM130 (Puthenveedu *et al.*, 2006). Thus, on the basis of our results, we conclude that GM130 acts primarily by mediating the homotypic tethering and coalescence of the tubulovesicular carriers and their incorporation into the stacks. However, we cannot formally exclude the possibility that GM130 might have an additional role in maintaining the Golgi ribbon by mediating the homotypic coalescence/fusion of neighboring *cis*-cisternae, as suggested by Puthenveedu *et al.* (2006); we simply cannot produce direct evidence for this role because of the technical limitations mentioned in resolving in time and space the trafficking events occurring within the crowded pericentrosomal Golgi area.

What we provide here is a further demonstration of how the structural organization of the GC can be heavily affected by the level of trafficking activity of the organelle, with a "resting" GC being composed of isolated stacks and the actively transporting GC being organized as a continuous ribbon-like organelle. However, the converse does not hold, because the functions of the GC, at least in terms of cargo transport and glycosylation, do not appear to absolutely require a fully organized ribbon. A large body of evidence indicates that indeed the transport of cargo to, through and out of the GC can occur under conditions in which the ribbon is interrupted (Cole *et al.*, 1996; Diao *et al.*, 2003; Trucco *et al.*, 2004) or even when the cisternal stacks are disorganized (Nagahama *et al.*, 2002; Kondylis and Rabouille, 2003; Zolov and Lupashin, 2005). Here, we have demonstrated that although knocking out GM130 induces

the breakdown of the Golgi ribbon, it also induces only a kinetic delay in the delivery of secretory cargo to the GC and does not affect the cargo at all in its progression through the disconnected stacks and in its glycosylation. In fact, our finding that the absence of a Golgi ribbon (induced by either depolymerizing the microtubules or interfering with GM130) does not correlate with a general defective posttranslational processing of exogenous and endogenous secretory cargos at the GC is in apparent discrepancy with the recent report by Puthenveedu *et al.* (2006), who concluded that the correct processing of some (unidentified) proteins is impaired when GM130 is knocked down with siRNAs. Explanations for these discrepancies may lie in the differences in the experimental systems used (as Puthenveedu *et al.*, 2006 used a stable HeLa cell line expressing GFP-GalNac-T2) and/or in the possibility that GM130 is required for the correct glycosylation of selected cargos. This would not be surprising, because there are known examples of cargo proteins that are able to physically interact with GM130 itself, or with the GM130 partners, such as GRASP65, p115 or the other golgins and that require this interaction for their transport along the secretory pathway (Kuo *et al.*, 2000; Roti *et al.*, 2002; Hosaka *et al.*, 2005; Bundis *et al.*, 2006; D'Angelo, Iodice, Marra, Beznoussenko, De Matteis, and Bonatti, unpublished data).

The finding that disruption of the Golgi ribbon has no major impact on the basic and conserved functions of the GC (i.e., cargo transport and glycosylation) prompts one to search for the reasons for the high degree of structural complexity of the mammal GC among the "higher order" functions of this organelle that are superimposed on and/or parallel to the basic and conserved ones. These include the ability of the mammalian GC to exert important regulatory functions during particular phases in the life of a cell, such as mitosis or apoptosis (Sutterlin *et al.*, 2002; Maag *et al.*, 2003; Hidalgo Carcedo *et al.*, 2004). Furthermore, the fragmentation of the Golgi ribbon induced by overexpression of GRASP65 impairs the polarized dendrite outgrowth in hippocampal neurons (Horton *et al.*, 2005). The latter example indicates that one of the roles of the Golgi ribbon is to ensure the targeted delivery of membranes to selected sites at the cell surface. A similar interpretation has been proposed for the reorientation of the GC toward the target cell in T lymphocytes during establishment of the immunological synapse or toward the leading edge of a cell during directional cell migration (Kupfer *et al.*, 1982, 1983).

Having positioned the primary site of action of GM130 at the morphofunctional level, what remains to be specified is the molecular mechanism by which GM130 exerts its actions. The original model, envisaging that GRASP65, GM130, p115, and giantin act as a tethering complex that bridges between vesicular and cisternal membranes (Shorter and Warren, 1999), has been revised recently, based on the evidence that in the presumed "bridging" component of the complex, p115, the binding sites for GM130 and giantin coincide (Linstedt *et al.*, 2000). Indeed, the interactions of GM130 and giantin with p115 have been shown to induce an open conformation of p115 and to facilitate the interaction with the small GTPase Rab1, rather than establishing a physical connection (Beard *et al.*, 2005). Thus, it is still possible that GM130 exerts its actions in a complex with these two proteins. However, the evidence that a truncated form of GM130 that lacks the p115 binding site can rescue the organization of the GC in GM130-knockout cells, whereas a truncated form of GM130 lacking the GRASP65-binding domain cannot, indicates that GRASP65, and not p115, is required for the activity of GM130 in maintaining the Golgi ribbon (Linstedt *et al.*, 2000). Here we show, however, that although required, the interaction with GRASP65 is by itself not sufficient for this activity of GM130. Indeed, a truncated form of GM130 lacking the 309 N-terminus amino acids (that thus lacks the first and half of the second coiled-coil domain, but that is still able to bind and relocalize GRASP65 to the GC) cannot carry out its role in the maintenance of GC structure. These results indicate that the integrity of the first and/or second coiled-coil domain of GM130 is required for its activity, and they suggest the involvement of a molecular partner of GM130 that specifically interacts with these domains. The likely candidates are YSK1, which binds the 75–271 region of GM130 (Preisinger *et al.*, 2004), and GM130 itself, which is known to homodimerize through its coiled-coil domains (Nakamura *et al.*, 1995). YSK1, a kinase that is activated in vitro by GM130 (Preisinger *et al.*, 2004) is likely to mediate some, but not all, of the effects induced by the GM130 knockout. Indeed, the pattern of GC fragmentation induced by the knockout of GM130 (i.e., disconnected, but central, Golgi elements) appears different from that described for the knockout of YSK1 or for the overexpression of a dominant-negative YSK1 (i.e., peripheral redistribution of the Golgi elements, or displacement from the centrosome of an intact Golgi ribbon, depending on the cells). Furthermore, the knockout of YSK1 does not affect the transport of VSVG, whereas we do see a delay in VSVG transport to the GC that is induced by the knock out of GM130. Thus, additional "properties" of the first coiled-coil domains of GM130 are relevant for its activity, such as, for instance, homodimerization. One can hypothesize that the dimerization in *trans* of GM130 may be part of the mechanism of tethering. This appears to be an interesting and likely possibility, also taking into account our observations that coalescence events occur much more frequently between two GM130-positive EGCs than between a GM130-positive and a GM130-negative EGC and that GM130 continuously cycles between EGCs and the *cis*-Golgi compartments (Marra *et al.*, 2001). Examples of interorganelle tethering operated by homodimerization in *trans* of coiled-coil molecules include the mitofusins and EEA1 (Mills *et al.*, 1999; Chen *et al.*, 2003), which mediate the tethering of mitochondria and early endosomes, respectively. In this context, interactors of GM130, such as p115 and Rab1, and possible others, would have regulatory roles for assuring the fidelity of the process.

Fully defining the composition, interactions and modes of action and regulation of the entire molecular network that is responsible for the structural organization of the GC remains a challenge for future investigations, and this will help us to unravel the "secret" functions that are promoted by such a complex architecture.

ACKNOWLEDGMENTS

The authors thank A. Luini and A. Colanzi for critical reading of the manuscript; all the colleagues who generously provided antibodies and constructs; M. Krieger for the ldlG cells; N. Martelli for the technical assistance with the FACS; C. P. Berrie for editorial assistance; and E. Fontana and R. Le Donne for the artwork. This work was supported by the Italian Association for Cancer Research (Milan, Italy) and Telethon Italia.

REFERENCES

Alvarez, C., Garcia-Mata, R., Hauri, H. P., and Sztul, E. (2001). The p115-interactive proteins GM130 and giantin participate in endoplasmic reticulum-Golgi traffic. J. Biol. Chem. *276*, 2693–2700.

Aridor, M., Bannykh, S. I., Rowe, T., and Balch, W. E. (1999). Cargo can modulate COPII vesicle formation from the endoplasmic reticulum. J. Biol. Chem. *274*, 4389–4399.

Aridor, M., Fish, K. N., Bannykh, S., Weissman, J., Roberts, T. H., Lippincott-Schwartz, J., and Balch, W. E. (2001). The Sar1 GTPase coordinates biosynthetic cargo selection with endoplasmic reticulum export site assembly. J. Cell Biol. *152*, 213–229.

Barnard, R. J., Morgan, A., and Burgoyne, R. D. (1997). Stimulation of NSF ATPase activity by alpha-SNAP is required for SNARE complex disassembly and exocytosis. J. Cell Biol. *139*, 875–883.

Beard, M., Satoh, A., Shorter, J., and Warren, G. (2005). A cryptic Rab1-binding site in the p115 tethering protein. J. Biol. Chem. *280*, 25840–25848.

Buccione, R., Bannykh, S., Santone, I., Baldassarre, M., Facchiano, F., Bozzi, Y., Di Tullio, G., Mironov, A., Luini, A., and De Matteis, M. A. (1996). Regulation of constitutive exocytic transport by membrane receptors. A biochemical and morphometric study. J. Biol. Chem. *271*, 3523–3533.

Bundis, F., Neagoe, I., Schwappach, B., and Steinmeyer, K. (2006). Involvement of Golgin-160 in cell surface transport of renal ROMK channel: co-expression of Golgin-160 increases ROMK currents. Cell Physiol. Biochem. *17*, 1–12.

Chen, H., Detmer, S. A., Ewald, A. J., Griffin, E. E., Fraser, S. E., and Chan, D. C. (2003). Mitofusins Mfn1 and Mfn2 coordinately regulate mitochondrial fusion and are essential for embryonic development. J. Cell Biol. *160*, 189–200.

Clermont, Y., Xia, L., Rambourg, A., Turner, J. D., and Hermo, L. (1993). Structure of the Golgi apparatus in stimulated and nonstimulated acinar cells of mammary glands of the rat. Anat. Rec. *237*, 308–317.

Cole, N. B., Smith, C. L., Sciaky, N., Terasaki, M., Edidin, M., and Lippincott-Schwartz, J. (1996). Diffusional mobility of Golgi proteins in membranes of living cells. Science *273*, 797–801.

Diao, A., Rahman, D., Pappin, D. J., Lucocq, J., and Lowe, M. (2003). The coiled-coil membrane protein golgin-84 is a novel rab effector required for Golgi ribbon formation. J. Cell Biol. *160*, 201–212.

Fritzler, M. J., Hamel, J. C., Ochs, R. L., and Chan, E. K. (1993). Molecular characterization of two human autoantigens: unique cDNAs encoding 95- and 160-kD proteins of a putative family in the Golgi complex. J. Exp. Med. *178*, 49–62.

Godi, A., Pertile, P., Meyers, R., Marra, P., Di Tullio, G., Iurisci, C., Luini, A., Corda, D., and De Matteis, M. A. (1999). ARF mediates recruitment of PtdIns-4-OH kinase-beta and stimulates synthesis of PtdIns(4,5)P2 on the Golgi complex. Nat. Cell Biol. *1*, 280–287.

Godi, A. *et al.* (1998). ADP ribosylation factor regulates spectrin binding to the Golgi complex. Proc. Natl. Acad. Sci. USA *95*, 8607–8612.

Griffiths, G., Fuller, S. D., Back, R., Hollinshead, M., Pfeiffer, S., and Simons, K. (1989). The dynamic nature of the Golgi complex. J. Cell Biol. *108*, 277–297.

Hidalgo Carcedo, C., Bonazzi, M., Spano, S., Turacchio, G., Colanzi, A., Luini, A., and Corda, D. (2004). Mitotic Golgi partitioning is driven by the membrane-fissioning protein CtBP3/BARS. Science *305*, 93–96.

Hobbie, L., Fisher, A. S., Lee, S., Flint, A., and Krieger, M. (1994). Isolation of three classes of conditional lethal Chinese hamster ovary cell mutants with temperature-dependent defects in low density lipoprotein receptor stability and intracellular membrane transport. J. Biol. Chem. *269*, 20958–20970.

Horton, A. C., Racz, B., Monson, E. E., Lin, A. L., Weinberg, R. J., and Ehlers, M. D. (2005). Polarized secretory trafficking directs cargo for asymmetric dendrite growth and morphogenesis. Neuron *48*, 757–771.

Hosaka, T., Brooks, C. C., Presman, E., Kim, S. K., Zhang, Z., Breen, M., Gross, D. N., Sztul, E., and Pilch, P. F. (2005). p115 Interacts with the GLUT4 vesicle protein, IRAP, and plays a critical role in insulin-stimulated GLUT4 translocation. Mol. Biol. Cell *16*, 2882–2890.

Jasmin, B. J., Cartaud, J., Bornens, M., and Changeux, J. P. (1989). Golgi apparatus in chick skeletal muscle: changes in its distribution during end plate development and after denervation. Proc. Natl. Acad. Sci. USA *86*, 7218–7222.

Klumperman, J. (2000). Transport between ER and Golgi. Curr. Opin. Cell Biol. *12*, 445–449.

Kondylis, V., and Rabouille, C. (2003). A novel role for dp115 in the organization of tER sites in *Drosophila*. J. Cell Biol. *162*, 185–198.

Kuo, A., Zhong, C., Lane, W. S., and Derynck, R. (2000). Transmembrane transforming growth factor-alpha tethers to the PDZ domain-containing, Golgi membrane-associated protein p59/GRASP55. EMBO J. *19*, 6427–6439.

Kupfer, A., Dennert, G., and Singer, S. J. (1983). Polarization of the Golgi apparatus and the microtubule-organizing center within cloned natural killer cells bound to their targets. Proc. Natl. Acad. Sci. USA *80*, 7224–7228.

Kupfer, A., Louvard, D., and Singer, S. J. (1982). Polarization of the Golgi apparatus and the microtubule-organizing center in cultured fibroblasts at the edge of an experimental wound. Proc. Natl. Acad. Sci. USA *79*, 2603–2607.

Linstedt, A. D., Jesch, S. A., Mehta, A., Lee, T. H., Garcia-Mata, R., Nelson, D. S., and Sztul, E. (2000). Binding relationships of membrane tethering components. The giantin N terminus and the GM130 N terminus compete for binding to the p115 C terminus. J. Biol. Chem. *275*, 10196–10201.

Losev, E., Reinke, C. A., Jellen, J., Strongin, D. E., Bevis, B. J., and Glick, B. S. (2006). Golgi maturation visualized in living yeast. Nature *441*, 1002–1006.

Maag, R. S., Hicks, S. W., and Machamer, C. E. (2003). Death from within: apoptosis and the secretory pathway. Curr. Opin. Cell Biol. *15*, 456–461.

Malmstrom, K., and Krieger, M. (1991). Use of radiation suicide to isolate constitutive and temperature-sensitive conditional Chinese hamster ovary cell mutants with defects in the endocytosis of low density lipoprotein. J. Biol. Chem. *266*, 24025–24030.

Marra, P., Maffucci, T., Daniele, T., Tullio, G. D., Ikehara, Y., Chan, E. K., Luini, A., Beznoussenko, G., Mironov, A., and De Matteis, M. A. (2001). The GM130 and GRASP65 Golgi proteins cycle through and define a subdomain of the intermediate compartment. Nat. Cell Biol. *3*, 1101–1113.

Marsh, B. J., Volkmann, N., McIntosh, J. R., and Howell, K. E. (2004). Direct continuities between cisternae at different levels of the Golgi complex in glucose-stimulated mouse islet beta cells. Proc. Natl. Acad. Sci. USA *101*, 5565–5570.

Matsuura-Tokita, K., Takeuchi, M., Ichihara, A., Mikuriya, K., and Nakano, A. (2006). Live imaging of yeast Golgi cisternal maturation. Nature *441*, 1007–1010.

Mills, I. G., Jones, A. T., and Clague, M. J. (1999). Regulation of endosome fusion. Mol. Membr. Biol. *16*, 73–79.

Mironov, A. A. *et al.* (2001). Small cargo proteins and large aggregates can traverse the Golgi by a common mechanism without leaving the lumen of cisternae. J. Cell Biol. *155*, 1225–1238.

Mironov, A. A. *et al.* (2003). ER-to-Golgi carriers arise through direct en bloc protrusion and multistage maturation of specialized ER exit domains. Dev. Cell *5*, 583–594.

Morin-Ganet, M. N., Rambourg, A., Deitz, S. B., Franzusoff, A., and Kepes, F. (2000). Morphogenesis and dynamics of the yeast Golgi apparatus. Traffic *1*, 56–68.

Nagahama, M., Usui, S., Shinohara, T., Yamaguchi, T., Tani, K., and Tagaya, M. (2002). Inactivation of Galpha(z) causes disassembly of the Golgi apparatus. J. Cell Sci. *115*, 4483–4493.

Nakamura, N., Lowe, M., Levine, T. P., Rabouille, C., and Warren, G. (1997). The vesicle docking protein p115 binds GM130, a cis-Golgi matrix protein, in a mitotically regulated manner. Cell *89*, 445–455.

Nakamura, N., Rabouille, C., Watson, R., Nilsson, T., Hui, N., Slusarewicz, P., Kreis, T. E., and Warren, G. (1995). Characterization of a cis-Golgi matrix protein, GM130. J. Cell Biol. *131*, 1715–1726.

Preisinger, C., Short, B., De Corte, V., Bruyneel, E., Haas, A., Kopajtich, R., Gettemans, J., and Barr, F. A. (2004). YSK1 is activated by the Golgi matrix protein GM130 and plays a role in cell migration through its substrate 14–3–3zeta. J. Cell Biol. *164*, 1009–1020.

Presley, J. F., Cole, N. B., Schroer, T. A., Hirschberg, K., Zaal, K. J., and Lippincott-Schwartz, J. (1997). ER-to-Golgi transport visualized in living cells. Nature *389*, 81–85.

Puthenveedu, M. A., Bachert, C., Puri, S., Lanni, F., and Linstedt, A. D. (2006). GM130 and GRASP65-dependent lateral cisternal fusion allows uniform Golgi-enzyme distribution. Nat. Cell Biol. *8*, 238–248.

Puthenveedu, M. A., and Linstedt, A. D. (2001). Evidence that Golgi structure depends on a p115 activity that is independent of the vesicle tether components giantin and GM130. J. Cell Biol. *155*, 227–238.

Roti, E. C., Myers, C. D., Ayers, R. A., Boatman, D. E., Delfosse, S. A., Chan, E. K., Ackerman, M. J., January, C. T., and Robertson, G. A. (2002). Interaction with GM130 during HERG ion channel trafficking. Disruption by type 2 congenital long QT syndrome mutations. Human Ether-a-go-go-Related Gene. J. Biol. Chem. *277*, 47779–47785.

Scales, S. J., Pepperkok, R., and Kreis, T. E. (1997). Visualization of ER-to-Golgi transport in living cells reveals a sequential mode of action for COPII and COPI. Cell *90*, 1137–1148.

Shorter, J., and Warren, G. (1999). A role for the vesicle tethering protein, p115, in the post-mitotic stacking of reassembling Golgi cisternae in a cell-free system. J. Cell Biol. *146*, 57–70.

Sonnichsen, B., Lowe, M., Levine, T., Jamsa, E., Dirac-Svejstrup, B., and Warren, G. (1998). A role for giantin in docking COPI vesicles to Golgi membranes. J. Cell Biol. *140*, 1013–1021.

Sutterlin, C., Hsu, P., Mallabiabarrena, A., and Malhotra, V. (2002). Fragmentation and dispersal of the pericentriolar Golgi complex is required for entry into mitosis in mammalian cells. Cell *109*, 359–369.

Trucco, A. *et al.* (2004). Secretory traffic triggers the formation of tubular continuities across Golgi sub-compartments. Nat. Cell Biol. *6*, 1071–1081.

Vasile, E., Perez, T., Nakamura, N., and Krieger, M. (2003). Structural integrity of the Golgi is temperature sensitive in conditional-lethal mutants with no detectable GM130. Traffic *4*, 254–272.

Zolov, S. N., and Lupashin, V. V. (2005). Cog3p depletion blocks vesicle-mediated Golgi retrograde trafficking in HeLa cells. J. Cell Biol. *168*, 747–759.